Journal of Quantitative Spectroscopy & Radiative Transfer 201 (2017) 53–63

Contents lists available at ScienceDirect

Journal of Quantitative Spectroscopy & Radiative Transfer

journal homepage: www.elsevier.com/locate/jqsrt

Transmittance of semitransparent windows with absorbing cap-shaped droplets condensed on their backside

Keyong Zhu [a], Laurent Pilon [b,*]

[a] Beihang University, School of Aeronautical Science and Engineering, No. 37, Xueyuan Road, Beijing 100191, China
[b] University of California, Los Angeles, Mechanical and Aerospace Engineering Department, 420 Westwood Plaza, Los Angeles, CA 90095-1597, USA

ARTICLE INFO

Article history:
Received 22 April 2017
Revised 20 May 2017
Accepted 14 June 2017
Available online 16 June 2017

Keywords:
Transmittance
Absorptance
Condensation
Greenhouses
Solar desalination

ABSTRACT

This study aims to investigate systematically light transfer through semitransparent windows with absorbing cap-shaped droplets condensed on their backside as encountered in greenhouses, solar desalination plants, photobioreactors and covered raceway ponds. The Monte Carlo ray-tracing method was used to predict the normal-hemispherical transmittance, reflectance, and normal absorptance accounting for reflection and refraction at the air/droplet, droplet/window, and window/air interfaces and absorption in both the droplets and the window. The droplets were monodisperse or polydisperse and arranged either in an ordered hexagonal pattern or randomly distributed on the backside with droplet contact angle θ_c ranging between 0 and 180° The normal-hemispherical transmittance was found to be independent of the spatial distribution of droplets. However, it decreased with increasing droplet diameter and polydispersity. The normal-hemispherical transmittance featured four distinct optical regimes for semitransparent window supporting nonabsorbing droplets. These optical regimes were defined based on contact angle and critical angle for internal reflection at the droplet/air interface. However, for strongly absorbing droplets, the normal-hemispherical transmittance (i) decreased monotonously with increasing contact angle for $\theta_c < 90°$ and (ii) remained constant and independent of droplet absorption index k_d, droplet mean diameter d_m, and contact angle θ_c for $\theta_c \geq 90°$ Analytical expressions for the normal-hemispherical transmittance were provided in the asymptotic cases when (1) the window was absorbing but the droplets were nonabsorbing with any contact angles θ_c, and (2) the droplets were strongly absorbing with contact angle $\theta_c > 90°$ Finally, the spectral normal-hemispherical transmittance of a 3 mm-thick glass window supporting condensed water droplets for wavelength between 0.4 and 5 μm was predicted and discussed in light of the earlier parametric study and asymptotic behavior.

1. Introduction

Several experimental measurements and numerical simulations have investigated the effects of water droplets condensed on the backside of glass or plastic windows on light transfer [1–8]. In general, dropwise condensation was found to decrease the transmittance of wet window for both visible and infrared radiation except for anti-drop (hydrophilic) surfaces [2–4]. In the photosynthetically active radiation (PAR) region (400–700 nm) - relevant to greenhouses [7] and microalgal culture systems [9] - reduction in transmittance is mainly due to the total internal reflection at the water droplet/air interfaces [1,10]. In the infrared region - relevant to solar desalination systems [11] - absorption by glass or plastic windows and water droplets plays a significant role in the transmittance reduction [6].

Recently, we investigated systematically the effects of nonabsorbing cap-shaped droplets condensed on the backside of transparent windows on their directional-hemispherical transmittance [10]. The latter was found to be independent of the size and spatial distributions of the droplets. Four optical regimes were identified in the normal-hemispherical transmittance as a function of contact angle θ_c and defined with respect to the critical angle θ_{cr} for total internal reflection at the droplet/air interface. The directional-hemispherical transmittance was nearly constant for droplet contact angle θ_c either smaller than the critical angle θ_{cr} (Regime I) or larger than 180°-θ_{cr} (Regime IV). However, for θ_c between θ_{cr} and 180°-θ_{cr}, the normal-hemispherical transmittance decreased rapidly with increasing θ_c to reach a minimum at 90° (Regime II) and increased rapidly with increasing θ_c up to 180°-θ_{cr} (Regime III). In addition, the normal-hemispherical transmittance decreased monotonously with increasing droplet projected surface area coverage for contact angle larger than θ_{cr}. However, for $\theta_c < \theta_{cr}$ (Regime I), the normal-hemispherical transmittance increased

* Corresponding author.
E-mail address: pilon@seas.ucla.edu (L. Pilon).

http://dx.doi.org/10.1016/j.jqsrt.2017.06.016
0022-4073/

Nomenclature

A	absorptance
d	droplet diameter, μm
d_m	mean diameter of droplets, μm
d_p	projected diameter of droplets, μm
f_A	droplet projected surface area coverage
f_N	frequency distribution of photons having passed through N droplets before being transmitted
H	thickness of the window, mm
j	imaginary unit
k	absorption index
l	path length of photon bundles, mm
l'	probable path length of photon bundles, mm
l_c	capillary length, μm
L	length of the window, mm
m	complex index of refraction
M	number of photon bundles
n	refractive index
$\mathbf{n}$	unit normal vector
N	effective refractive index
$\mathbf{p}$	position vector of photon bundles
r	reflection coefficient
R	reflectance
R_l	random number
$\mathbf{s}$	unit vector of photon bundle directions
W	width of the window, mm

Greek symbols

θ_c	contact angle, °
θ_{cr}	critical angle, °
φ	azimuthal angle, °
λ	wavelength, μm
ρ	interface reflectance
κ	absorption coefficient, μm^{-1}
$\tilde{\kappa}$	effective absorption coefficient, μm^{-1}
τ	transmissivity
σ	standard deviation of droplet diameter, μm

Subscripts

i	incident
r	reflected
t	transmitted
a	air
w	window
d	droplet
f	film
dh	directional-hemispherical
nh	normal-hemispherical
λ	spectral
$\perp$, $\parallel$	perpendicular and parallel polarized radiation

slightly with increasing droplet projected surface area coverage. Finally, experimental measurements and numerical simulations of light transfer in transparent or semitransparent windows supporting nonabsorbing or absorbing droplets were reviewed in details in our recent study [10] and need not be repeated.

The present paper extends our previous study [10] to situations when the condensed cap-shaped droplets and/or the window are absorbing. Here also, the effects of (i) droplets' spatial arrangement and (ii) size distribution, (iii) incident angle, (iv) complex index of refraction of the window and (v) the droplets, and (vi) contact angle were systematically investigated. The results could be used for the design, material selection, and thermal management of greenhouses, solar desalination, and photobioreactor systems.

2. Analysis

2.1. Problem statement

Figs. 1(a) and 1(b) show the top and side views of the simulated polydisperse droplets randomly distributed on the back window with length L, width W, and thickness H. The window was exposed to collimated monochromatic radiation of wavelength λ incident on its front face at a polar angle θ_i. Photons were reflected, transmitted, or absorbed by the semitransparent window with refractive and absorption indices denoted by n_w and k_w, respectively. Part of the incident radiation was transmitted through the back face of the window into the droplets of refractive and absorption indices denoted by n_d and k_d, respectively. Then, radiation could be (i) internally reflected within the droplet, (ii) transmitted through the droplet/air interface or the droplet/window interface, or (iii) absorbed by the droplets. In the present study, the dimensions of the window for simulating randomly distributed monodisperse or polydisperse droplets were $L = W = 5$ mm, and $H = 3$ mm. The refractive and absorption indices of the surrounding air were taken as $n_a = 1.0$ and $k_a = 0$.

2.2. Assumptions

To make the problem mathematically tractable, several assumptions were made in our simulations:

1. All interfaces were optically smooth so that all reflections were specular and the generalized Snell's law and Fresnel's equations were valid.
2. The droplets were cap-shaped with a constant curvature and diameter d much smaller than the capillary length l_c, i.e., $d \ll l_c$ [12]. For water droplets in air, l_c equals 2.7 mm [10]. Here, the droplets diameter d was smaller than 270 μm to satisfy $d \ll l_c$ [10].
3. The dimensions of the window and droplets were much larger than the radiation wavelength so geometric optics prevailed and interferences and other wave effects could be ignored.
4. The boundary conditions on the sides of the window were periodic.

The generalized Snell's law for reflection and refraction at the interface between two adjacent absorbing media, referred to by subscript "i" (incident side of the interface) and "t" (transmitted side) with respective complex index of refraction $m_i = n_i - \mathrm{j}k_i$ and $m_t = n_t - \mathrm{j}k_t$ where $\mathrm{j}^2 = -1$, can be written as [13–15]

$$N_i \sin\theta_i = N_i \sin\theta_r = N_t \sin\theta_t. \tag{1}$$

Here, θ_i, θ_r, and θ_t are respectively the angles of the incident, reflected, and transmitted radiations defined according to

$$\mathbf{s}_r = \mathbf{s}_i - 2\cos\theta_i \mathbf{n}, \tag{2}$$

$$\mathbf{s}_t = \mathbf{s}_i N_i/N_t + (\cos\theta_t - \cos\theta_i N_i/N_t)\mathbf{n}. \tag{3}$$

The unit vectors $\mathbf{s}_i$, $\mathbf{s}_r$, and $\mathbf{s}_t$ represent the incident, reflected, and transmitted directions while $\mathbf{n}$ is the unit normal vector to the interface pointing towards the transmitted medium (see Fig. S1 in Supplementary Material). The effective refractive indices N_i and N_t of the media on the incident and transmitted sides of the interface are respectively defined as [13–15]

$$N_i^2 = \frac{1}{2}\left[\sqrt{\left(n_i^2 - k_i^2\right)^2 + \left(2n_i k_i/\cos\theta_i\right)^2} + \left(n_i^2 - k_i^2\right)\right], \tag{4}$$

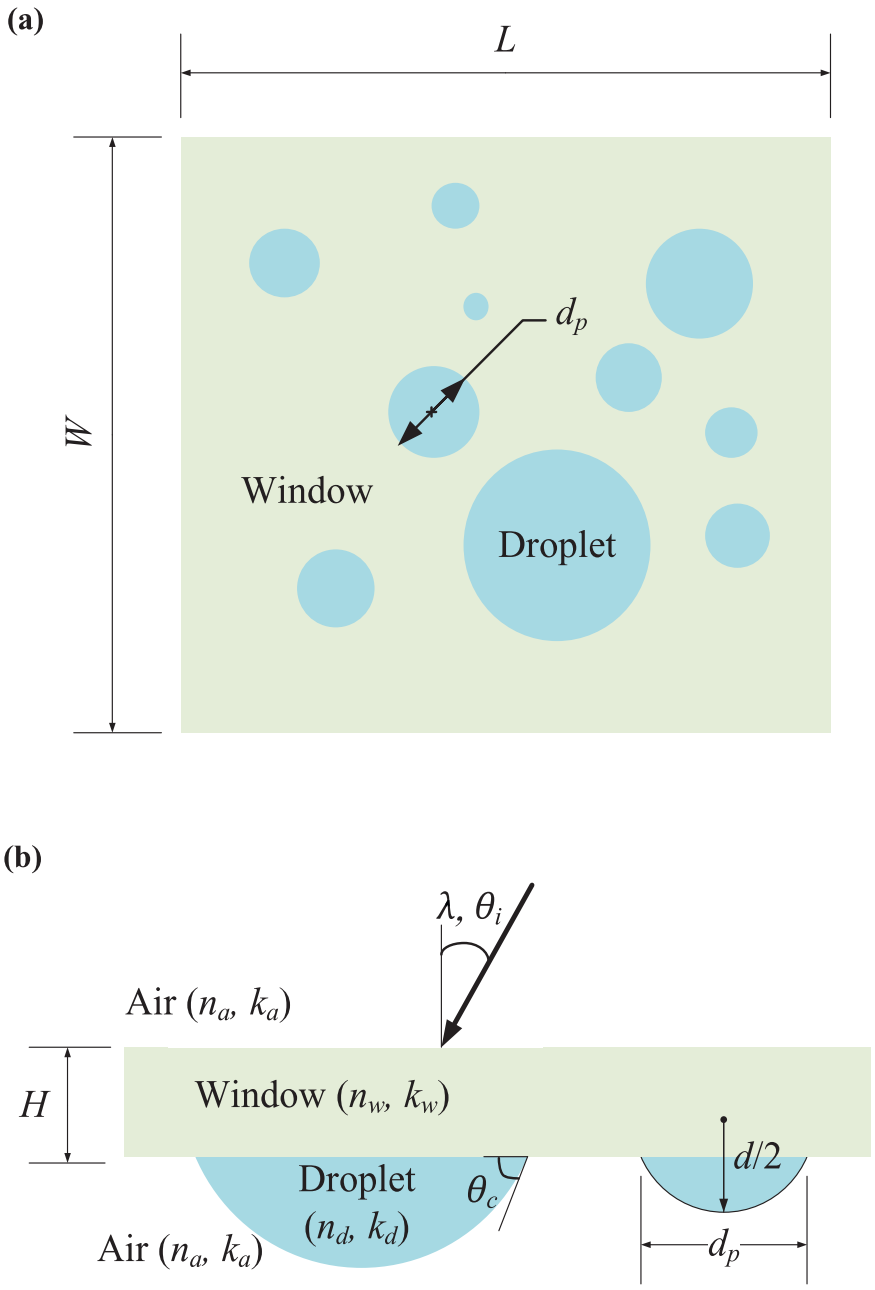

Fig. 1. (a) Top view of the semitransparent window (n_w, k_w) of dimensions $L \times W \times H$ supporting polydisperse absorbing cap-shaped droplets (n_d, k_d) with contact angle θ_c, diameter d, and projected diameter d_p. (b) Cross-section of the semitransparent window supporting absorbing droplets exposed to collimated incident radiation at angle θ_i with the wavelength λ.

$$N_t^2 = \frac{1}{2}\left[\sqrt{\left(n_t^2 - k_t^2 - N_i^2\sin^2\theta_i\right)^2 + 4n_t^2k_t^2} + \left(n_t^2 - k_t^2 + N_i^2\sin^2\theta_i\right)\right]. \tag{5}$$

Note that total internal reflection occurs when the incident angle θ_i is larger than the critical angle θ_{cr} defined as $\theta_{cr} = \sin^{-1}(N_i/N_t)$ where $N_t \geq N_i$ [13–15]. In addition, the effective absorption indices K_i and K_t can be expressed as [13–15]

$$K_{i/t} = n_{i/t}k_{i/t}/\left(N_{i/t}\cos\theta_{i/t}\right). \tag{6}$$

Moreover, the generalized Fresnel's equations give the reflection coefficients for the perpendicular and parallel polarized radiations, respectively denoted by $r_\perp$ and $r_\parallel$, defined as [13,15]

$$r_\perp = \frac{(N_i\cos\theta_i - jK_i) - (N_t\cos\theta_t - jK_t)}{(N_i\cos\theta_i - jK_i) + (N_t\cos\theta_t - jK_t)}, \tag{7}$$

$$r_\parallel = \frac{m_t^2\ (N_i\cos\theta_i - jK_i) - m_i^2\ (N_t\cos\theta_t - jK_t)}{m_t^2\ (N_i\cos\theta_i - jK_i) + m_i^2\ (N_t\cos\theta_t - jK_t)}. \tag{8}$$

In addition, the reflectance ρ of the interface between two absorbing media exposed to unpolarized radiation can be written as [13–15]

$$\rho = (|r_\perp|^2 + |r_\parallel|^2)/2. \tag{9}$$

Finally, for an absorbing medium, the transmissivity τ_j along the path length l_j in medium "j" is given by [14,15]

$$\tau_j = \exp\left[-\left(4\pi k_j/\lambda\right)\left(n_j/N_j\right)l_j\right]. \tag{10}$$

2.3. Monte Carlo ray-tracing method

Monte Carlo ray-tracing method [16,17] was used to predict the directional-hemispherical reflectance, transmittance, and absorptance of a semitransparent window exposed to collimated radiation and supporting absorbing cap-shaped droplets condensed on its backside. The methodology used to generate randomly distributed and polydisperse droplets on the window was previously discussed [10] and need not be repeated. The incident photon bundles may experience multiple reflection and refraction at the window/air, window/droplet, and droplet/air interfaces, as well as absorption in either the window or the droplets. The photon bundles were traced until (i) they reached either the imaginary surface above the dry front surface of the window, when they were counted as reflected, (ii) they reached the imaginary surface beyond the droplets, when they were counted as transmitted, or (iii) they were absorbed by either the window or the droplets. Fig. 2 shows the block diagram of the Monte Carlo ray-tracing algorithm implemented for a single photon bundle. The computational steps were as follows:

(1) For a given incident angle θ_i, determine the random position vector $\mathbf{p}_0 = (x_0, y_0)$ in the x-y plane of the front (dry) window where the incident photons reached the window.
(2) Determine the random incident direction $\mathbf{s}_i$ defined by a specific polar angle θ_i and a random azimuthal angle φ_i.
(3) Calculate the reflectance ρ of the air/window interface based on generalized Fresnel's equations [Eqs. (4)–(9)]. Generate a random number between 0 and 1 obeying uniform distribution. If the random number is smaller than ρ, then reflection occurs, otherwise, refraction occurs.
(4) Determine the specular reflection and refraction directions $\mathbf{s}_r$ or $\mathbf{s}_t$ from generalized Snell's law [Eqs. (1)–(3)].
(5) Calculate the position $\mathbf{p}'$ of the next interface reached by the photon bundle based on geometric configurations. Periodic boundary conditions prevailed on the four vertical sides of the window, taken as horizontal (Fig. 1). Indeed, when the photon bundle reached one of the vertical sides of the window, it reentered the window on the opposite vertical side at the same height and in the same direction.
(6) Calculate the distance $l_{w/d}$ traveled by the photon bundle through the window (subscript "w") or the droplet (subscript "d") from previous position $\mathbf{p}_0$ to present position $\mathbf{p}'$ in the window or the droplets. Generate a random number R_l between 0 and 1 obeying uniform distribution to calculate the probable path length $l'_{w/d}$ in the window or the droplets given by [16,17]

$$l'_{w/d} = -ln\, R_l/\tilde{\kappa}_{w/d}, \tag{11}$$

where the effective absorption coefficient is expressed as [14,15]

$$\tilde{\kappa}_{w/d} = (4\pi k_{w/d}/\lambda)(n_{w/d}/N_{w/d}). \tag{12}$$

If $l_{w/d} > l'_{w/d}$, the photon was absorbed and the number of absorbed photon bundles M_A was incremented by 1. Then, the ray-tracing procedure ended for the traced photon bundle and the procedure restarted at Step 1 for a new photon bundle. If $l_{w/d} < l'_{w/d}$, the photon was not absorbed and reached the next interface at location $\mathbf{p}'$.
(7) Reset the initial location to $\mathbf{p}_0 = \mathbf{p}'$ and directions $\mathbf{s}_i = \mathbf{s}_r$ or $\mathbf{s}_i = \mathbf{s}_t$. Then repeat Steps 3–6.

Whenever the updated position $\mathbf{p}_0$ was above the dry front side of the window, it indicated that the photon was reflected and the number of reflected photon bundles M_R was incremented by 1. Similarly, if the position $\mathbf{p}_0$ was beyond all droplets, it meant that the photon was transmitted and the number of transmitted photon bundles M_T was incremented by 1. Then, the ray-tracing procedure ended for the traced photon bundle and the procedure restarted for a new photon bundle at Step 1.

Finally, after tracing M statistically significant number of photon bundles, the directional-hemispherical transmittance T_{dh}, the directional-hemispherical reflectance R_{dh}, and the directional absorptance A_d of the wet window were calculated according to

$$T_{dh} = M_T/M, \quad R_{dh} = M_R/M, \quad \text{and} \quad A_d = M_A/M. \tag{13}$$

Here, from energy conservation principles, $M = M_T + M_R + M_A$, or $T_{dh} + R_{dh} + A_d = 1$. In all simulation results reported in this study, the total number of photon bundles simulated was $M = 10^6$ was sufficient to achieve numerical convergence.

2.4. Validation

Fig. 3(a) plots the directional transmittance of a semitransparent window ($n_w = 1.5$, $k_w = 10^{-5}$) of thickness $H_w = 3$ mm without or with a semitransparent liquid film ($n_f = 1.33$, $k_f = 10^{-3}$) of thickness $H_f = 50\,\mu$m for incident wavelength $\lambda = 1\,\mu$m predicted by our Monte Carlo ray tracing algorithm. Analytical expressions for the directional transmittance of a window without or with a film, denoted by T_w and T_{wf}, can be written as [16]

$$T_w = \frac{(1-\rho_{aw})^2\tau_w}{1-\rho_{aw}^2\tau_w^2}, \tag{14}$$

$$T_{wf} = \frac{(1-\rho_{aw})(1-\rho_{wf})(1-\rho_{fa})\tau_w\tau_f}{(1-\rho_{aw}\rho_{wf}\tau_w^2)(1-\rho_{wf}\rho_{fa}\tau_f^2) - (1-\rho_{wf})^2\rho_{aw}\rho_{fa}\tau_w^2\tau_f^2}, \tag{15}$$

where ρ_{aw}, ρ_{wf}, and ρ_{fa} are the specular reflectivities at the air/window, window/film, and film/air interfaces respectively given by Eqs. (4)–(9). The transmissivities τ_w and τ_f of the window and film were given by Eq. (10) with the associated path lengths were $l_w = H_w/\cos\theta_w$ and $l_f = H_f/\cos\theta_f$, respectively. Fig. 3(a) shows excellent agreement between our numerical simulations and predictions by the above analytical expressions for both transmittances T_w and T_{wf}.

Moreover, the normal-hemispherical reflectance of a semitransparent glass window with a single absorbing water droplet condensed on its backside was predicted and compared with those reported in Ref. [1]. The glass window thickness was $H_w = 1.1$ mm and the projected droplet diameter was $d_p = 50\,\mu$m. The incident wavelength was $\lambda = 650$ nm. The refractive index of the window and droplets were respectively taken as $n_w = 1.5$ and $n_d = 1.33$ while their absorption coefficients were assumed to be the same and equal to $\kappa_{w,\lambda} = 4\pi k_{w,\lambda}/\lambda = 0.04\ \text{mm}^{-1}$ and $\kappa_{d,\lambda} = 4\pi k_{d,\lambda}/\lambda = 0.04\ \text{mm}^{-1}$. Fig. 3(b) compares the normal-hemispherical reflectance as a function of contact angle obtained by our study with simulation results reported in Ref. [1]. Here also, excellent agreement was observed.

Overall, these different cases confirmed the validity of our algorithm and the proper consideration of the different optical phenomena and boundary conditions. Finally, for all simulations reported in this manuscript, it was systematically verified that energy was conserved, i.e., $T_{dh} + R_{dh} + A_d = 1$.

3. Results and discussion

Sections 3.1–3.4 present a parametric study for arbitrary window materials and droplet fluid with realistic optical properties assumed to be wavelength-independent. More specifically, the wavelength and refractive indices of the window and droplets were arbitrarily set as $\lambda = 1\,\mu$m, $n_w = 1.5$ and $n_d = 1.33$, respectively.

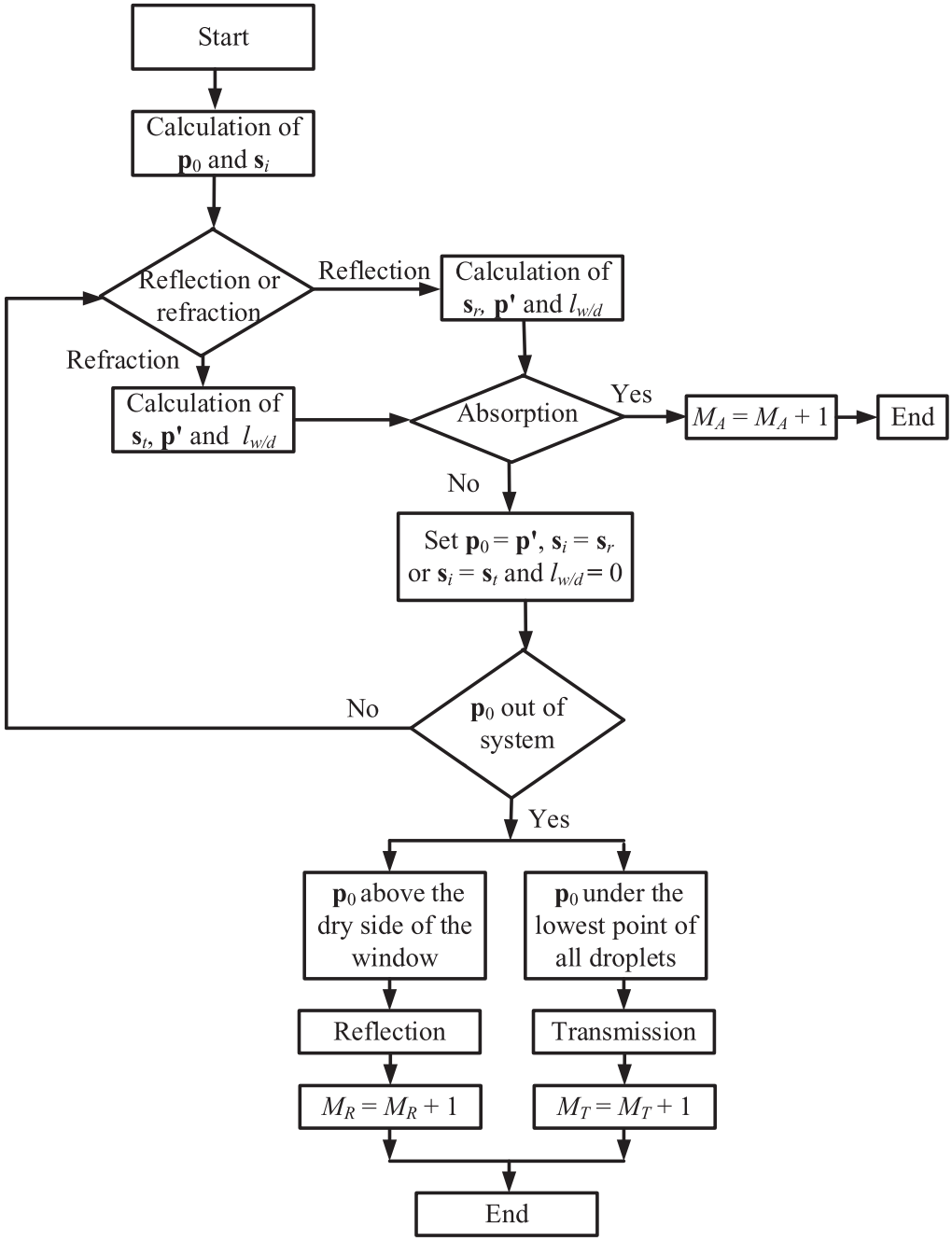

Fig. 2. Block diagram of the Monte Carlo ray-tracing algorithm for a single photon bundle. $\mathbf{p}_0$ ($\mathbf{p}'$) was the position where the photon bundle reached the interface, and $\mathbf{s}_i$, $\mathbf{s}_r$ and $\mathbf{s}_t$ were the incident, reflection, and transmission directions, respectively. $l_{w/d}$ was the distance traveled by the photon bundle between the previous position $\mathbf{p}_0$ to the present position $\mathbf{p}'$ in the window or droplets.

Section 3.5 considered the practical case of a soda-lime silicate glass window supporting condensed water droplets on its backside in the spectral range of practical interest to applications previously mentioned. The spectral refractive and absorption indices for wavelength λ ranging between 400 nm and 5 μm were taken (i) from Ref. [18] for soda-lime silicate glass ($n_{w,\lambda}$, $k_{w,\lambda}$), and (ii) from Ref. [19] for water ($n_{d,\lambda}$, $k_{d,\lambda}$) (see Fig. S2 in Supplementary Material).

3.1. Effect of droplet spatial and size distributions

Fig. 4 shows the normal-hemispherical transmittance as a function of contact angle θ_c for (a) a semitransparent window ($n_w = 1.5$, $k_w = 10^{-5}$) with nonabsorbing droplets ($n_d = 1.33$, $k_d = 0$) and (b) a transparent window ($n_w = 1.5$, $k_w = 0$) with absorbing droplets ($n_d = 1.33$, $k_d = 10^{-3}$) with droplet projected surface area coverage $f_A = 30\%$. Three configurations were considered namely (i) monodisperse droplets arranged in an ordered hexagonal pattern, (ii) monodisperse and randomly distributed droplets, and (iii) polydisperse and randomly distributed droplets following a normal distribution with mean diameter d_m and standard deviation σ such that $d_m - \sigma < d < d_m + \sigma$. The droplets' mean diameter d_m ranged between 50 and 250 μm. Fig. 4(a) indicates that, for nonabsorbing droplets, the normal-hemispherical transmittance of the semitransparent window was independent of both the droplet spatial and size distributions including their mean diameter d_m. In addition, Fig. 4(b) establishes that the droplet spatial distribution

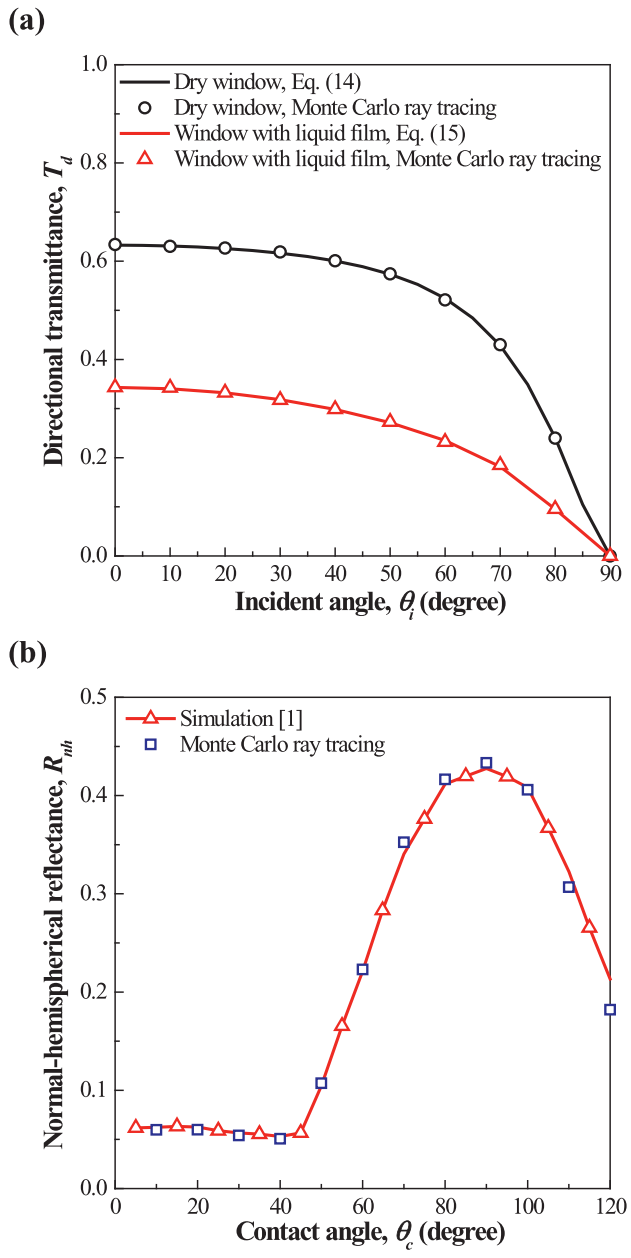

Fig. 3. (a) Comparison of predictions by Monte Carlo ray tracing and Eqs. (14) and (15) for the directional transmittance, as a function of incident angle θ_i at incident wavelength $\lambda = 1\ \mu$m, for a semitransparent window ($n_w = 1.5$, $k_w = 10^{-5}$) of thickness $H_w = 3$ mm without and with a semitransparent film ($n_f = 1.33$, $k_f = 10^{-3}$) of thickness $H_f = 50\ \mu$m. (b) Comparison of the normal-hemispherical reflectance of a glass window with a single absorbing cap-shaped droplet as a function of contact angle θ_c reported in Ref. [1] and those predicted in the presented study for glass window thickness $H_w = 1.1$ mm, droplet projected diameter $d_p = 50\ \mu$m, incident wavelength $\lambda = 650$ nm, refractive index of glass window and water droplets $n_w = 1.5$ and $n_d = 1.33$, and absorption coefficient for both glass and water $\kappa_{w,\lambda} = \kappa_{d,\lambda} = 0.04$ mm^{-1}.

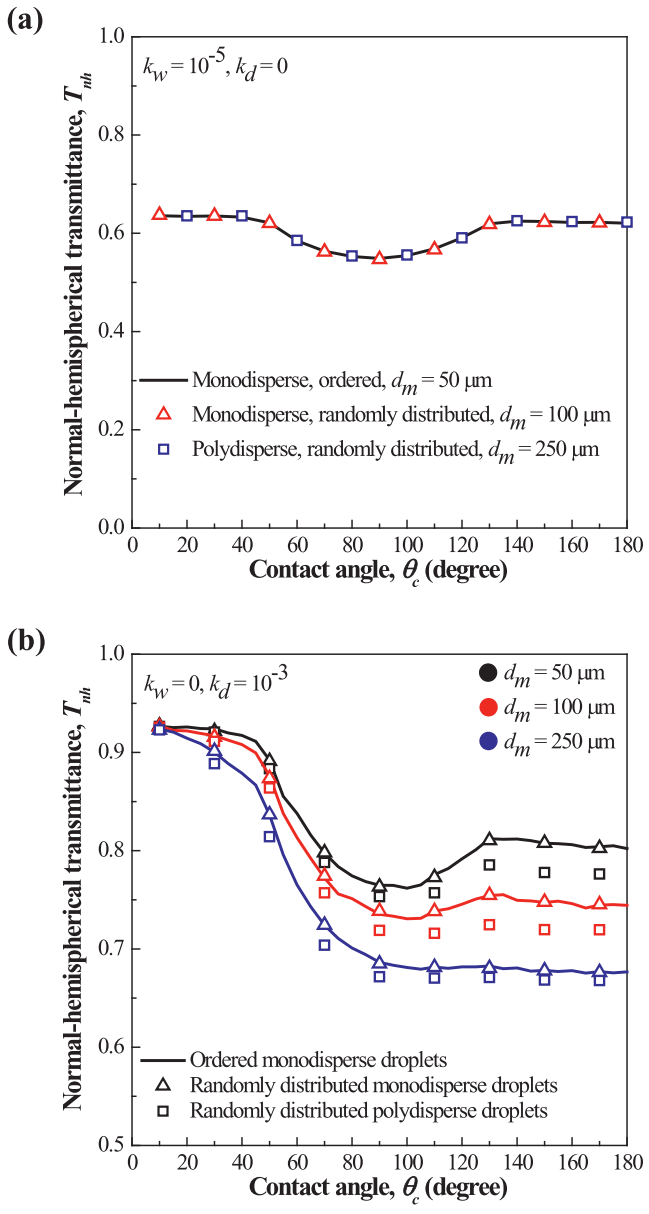

Fig. 4. Effect of droplet spatial distribution and size distribution on the normal-hemispherical transmittance for (a) a semitransparent window ($k_w = 10^{-5}$) and non-absorbing droplets ($k_d = 0$), and (b) a transparent window ($k_w = 0$) and absorbing droplets ($k_d = 10^{-3}$), with $f_A = 30\%$, $\lambda = 1\ \mu$m, $n_w = 1.5$ and $n_d = 1.33$. The diameter of polydisperse droplets was such that $d_m - \sigma < d < d_m + \sigma$, where $d_m = \sigma$.

had a slight effect on the normal-hemispherical transmittance of the transparent window with absorbing droplets. However, the normal-hemispherical transmittance decreased significantly with increasing absorbing droplet mean diameter d_m. This was due to the fact that, for a given droplet projected surface area coverage f_A, the larger the mean diameter d_m the larger the overall volume of liquid suspended on the window which resulted in stronger absorption of the radiation by the droplets. For the same reasons, the droplet polydispersity also reduced the normal-hemispherical transmittance T_{nh} compared with monodisperse droplets, for a given value of f_A. This reduction in T_{nh} was particularly apparent for contact angles larger than 90°

3.2. Effect of window and droplet absorption index

Fig. 5 plots the normal-hemispherical transmittance as a function of contact angle θ_c for (a) a semitransparent window ($n_w = 1.5$) with different absorption index k_w with nonabsorbing droplets ($n_d = 1.33$, $k_d = 0$), and for a transparent window ($k_w = 0$) with monodisperse droplets of diameter (b) $d_m = 50\ \mu$m, (c) $d_m = 100\ \mu$m, and (d) $d_m = 250\ \mu$m with absorption index k_d ranging between 0 and 5×10^{-2} and incident wavelength $\lambda = 1\ \mu$m. Here, the droplet projected surface area coverage was $f_A = 55\%$ corresponding to the equilibrium coverage of a vertical window [1].

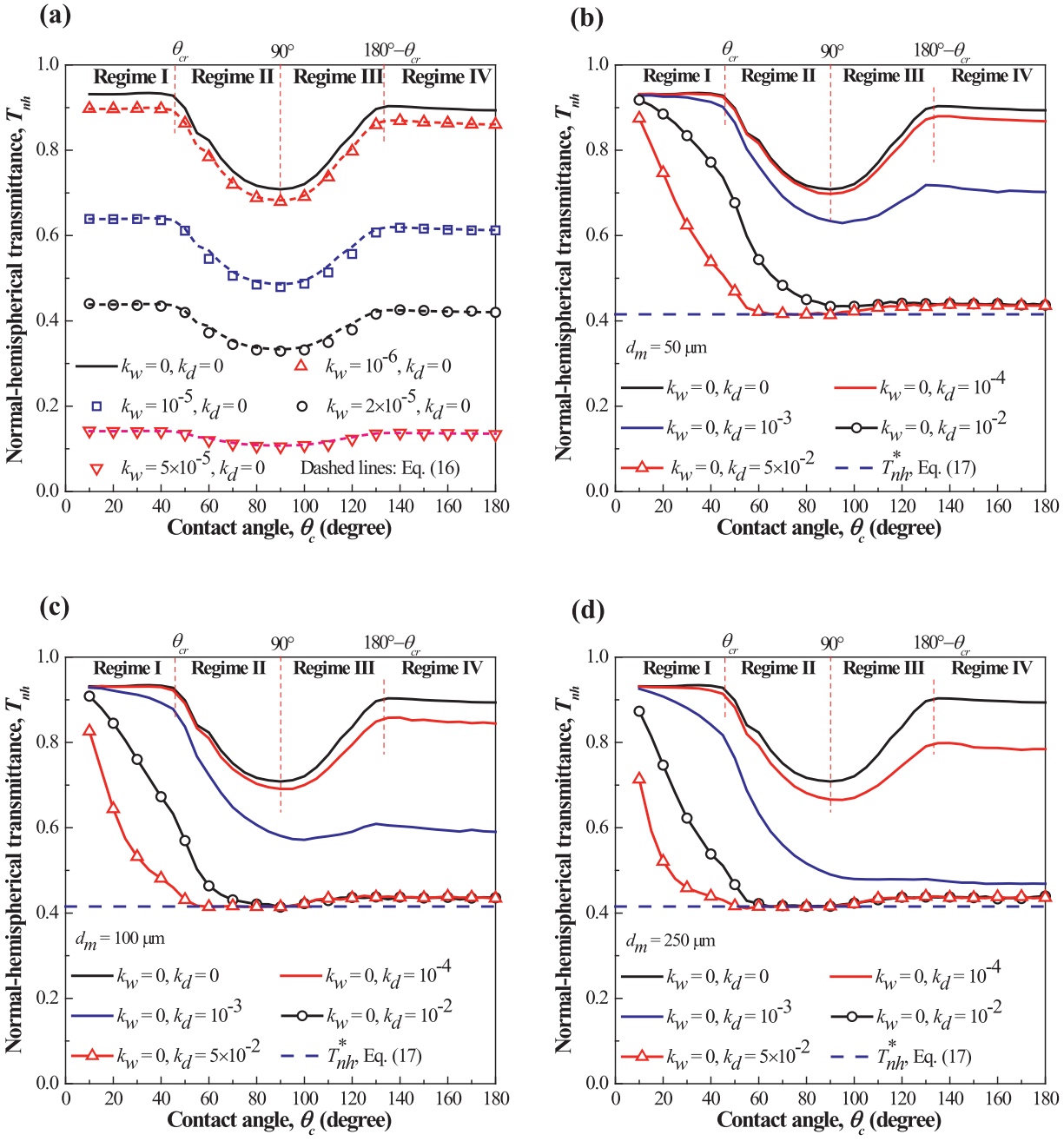

Fig. 5. Effect of contact angle on the normal-hemispherical transmittance for (a) a semitransparent window with different absorption index k_w and nonabsorbing droplets ($k_d = 0$), and for a transparent window ($k_w = 0$) and absorbing droplets with different absorption index k_d and (b) $d_m = 50\,\mu$m, (c) $d_m = 100\,\mu$m, and (d) $d_m = 250\,\mu$m. The droplets were monodisperse and arranged in an ordered hexagonal pattern with $f_A = 55\%$, $\lambda = 1\,\mu$m, $n_w = 1.5$ and $n_d = 1.33$.

Fig. 5(a) indicates that the normal-hemispherical transmittance for transparent windows and nonabsorbing droplets (i.e., $k_w = 0$ and $k_d = 0$) featured four optical regimes defined with respect to the critical angle θ_{cr} for total internal reflection at droplet/air interface, as previously established [10] and summarized in Introduction. The same four regimes could be observed for slightly absorbing window and nonabsorbing droplets ($k_w = 10^{-6}$–5×10^{-5} and $k_d = 0$) albeit with a smaller normal-hemispherical transmittance compared with that for $k_w = 0$ and $k_d = 0$. However, for more strongly absorbing window ($k_w > 5\times10^{-5}$ and $k_d = 0$), the normal-hemispherical transmittance became less and less sensitive to droplet contact angle θ_c. This can be attributed to the fact that most photons were absorbed in the window and droplets had a decreasing influence on transmittance. For any contact angle, the normal-hemispherical transmittance satisfied the relationship

$$T_{nh}(k_w, \vartheta_c) \approx T_{nh}(k_w = 0, \vartheta_c)\exp(-\tilde{\kappa}_w H_w). \quad (16)$$

where the argument $\tilde{\kappa}_w H_w$ of the exponential function represents the window optical thickness. Fig. 5(a) establishes that the normal-hemispherical transmittance T_{nh} obtained from Monte Carlo simulations was in excellent agreement with predictions by Eq. (16).

Similarly, Fig. 5(b) indicates that for transparent window and slightly absorbing droplets ($k_w = 0$ and $k_d = 10^{-4}$), the same four regimes could be observed albeit with a smaller normal-hemispherical transmittance, particularly for contact angle larger than 90° However, for strongly absorbing droplets ($k_w = 0$ and $k_d \geq 10^{-2}$), the four optical regimes were no longer apparent. Instead, the normal-hemispherical transmittance decreased with in-

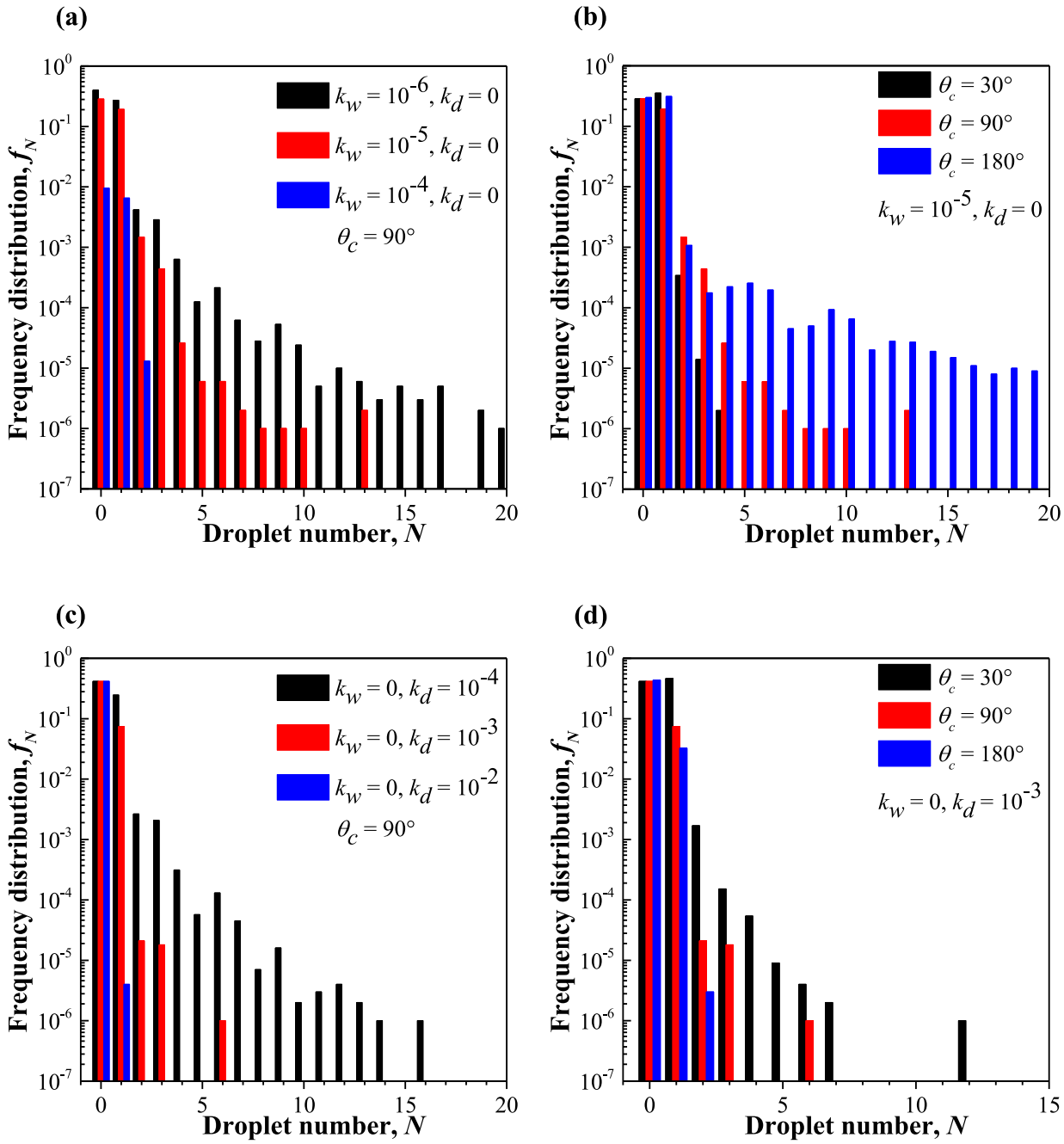

Fig. 6. Frequency distribution of transmitted photon bundles as a function of droplets number photon bundles passed through at normal incidence, i.e., $\theta_i = 0°$ (a) Effect of a semitransparent window with different absorption index k_w and nonabsorbing droplets ($k_d = 0$) (b) Effect of contact angle for a semitransparent window and nonabsorbing droplets. (c) Effect of a transparent window ($k_w = 0$) and absorbing droplets with different absorption index k_d. The droplets were monodisperse and arranged in an ordered hexagonal pattern with $d_m = 250\ \mu$m, $f_A = 55\%$, $\lambda = 1\ \mu$m, $n_w = 1.5$ and $n_d = 1.33$.

creasing contact angle for $\theta_c < 90°$ and remained constant and independent of absorption index k_d, droplet mean diameter d_m, and contact angle θ_c for $\theta_c \geq 90°$ [Figs. 5(b)–5(d)]. This was due to the fact that all photons entering the strongly absorbing droplets were absorbed. Then, the normal-hemispherical transmittance of the wet window could be expressed as the product of the normal-normal transmittance T_w of the dry window and the surface area fraction of the window $(1 - f_A)$ not covered by the projected droplets, i.e.,

$$T_{nh}^{*} \approx T_w(1 - f_A). \tag{17}$$

Figs. 5(b)–5(d) show excellent agreement between results of T_{nh} obtained by Monte Carlo ray tracing simulations and predictions by Eq. (17) for $k_w = 0$ and $k_d \geq 10^{-2}$ and $\theta_c \geq 90°$, for all values of mean diameter d_m and projected surface area coverage f_A considered.

3.3. Transmitted photons passing through multiple droplets

Fig. 6 shows the frequency distribution f_N of photon bundles having passed through N droplets before being transmitted, under normal incidence, as a function of N (a) for semitransparent windows with absorption index k_w in the range 10^{-6}–10^{-4} and nonabsorbing droplets ($k_d = 0$) with $\theta_c = 90°$, (b) for semitransparent windows with nonabsorbing droplets ($k_w = 10^{-5}$ and $k_d = 0$) for contact angle $\theta_c = 30°$, 90°, and 180°, (c) for transparent win-

dows ($k_w = 0$) but absorbing droplets with absorption index k_d in the range 10^{-4}–10^{-2} and $\theta_c = 90°$, and (d) for transparent windows and absorbing droplets ($k_w = 0$ and $k_d = 10^{-3}$) with different contact angle θ_c. In all cases, the droplets were monodisperse and arranged in an ordered hexagonal pattern with $d_m = 250\,\mu$m and $f_A = 55\%$ while $\lambda = 1\,\mu$m, $n_w = 1.5$, and $n_d = 1.33$.

Fig. 6(a) indicates that for slightly absorbing window ($k_w = 10^{-6}$), 40% of the transmitted photon bundles passed directly through the window while 27% passed through a single droplet. For the more strongly absorbing window ($k_w = 10^{-5}$), these frequencies decreased to 28% and 19%, respectively. In the limiting case of a strongly absorbing window (e.g., $k_w = 10^{-4}$ or larger), no photon was transmitted through the wet window, i.e., $T_{dh} = 0$. The maximum number of droplets through which transmitted photon bundles passed decreased from 29, 13, to 2 as the window absorption index increases from $k_w = 10^{-6}$, 10^{-5}, to 10^{-4}, respectively.

Fig. 6(b) indicates that, for semitransparent window ($k_w = 10^{-5}$) and nonabsorbing droplets ($k_d = 0$), 28%, 28%, and 30% of the transmitted photon bundles did not pass through any droplet (i.e., $N = 0$) for contact angle θ_c equals to 30°, 90°, and 180°, respectively. On the other hand, the frequency of transmitted photon bundles passing through a single droplet was 35%, 19%, and 31% for contact angle $\theta_c = 30°$, 90°, and 180°, respectively. The difference could be attributed to total internal reflection within the droplets which resulted in photons being back-scattered for $\theta_c = 90°$ (Regime II), and forward scattered for $\theta_c = 180°$ (Regime IV). In addition, the maximum number of droplets through which transmitted photon bundles passed increased with contact angle and was 4, 13, and 92 for $\theta_c = 30°$, 90°, and 180°, respectively.

Fig. 6(c) indicates that, for transparent windows, surface coverage $f_A = 55\%$, and contact angle $\theta_c = 90°$, 42% of the transmitted photon bundles did not pass through any droplets for any values of droplet absorption index k_d. However, the number of photons passing through one or more droplets decreased sharply with increasing k_d due to absorption in the droplets. In fact, 25%, 7%, and ~0% of the transmitted photon bundles passed through one droplet with the maximum number of droplets decreasing from 16, 6, to 1 as k_d increased from 10^{-4}, 10^{-3}, to 10^{-2}, respectively.

Fig. 6(d) indicates that for transparent window ($k_w = 0$) with absorbing droplets ($k_d = 10^{-3}$) covering $f_A = 55\%$ of the window back surface, the frequencies of transmitted photon bundles that did not pass through any droplets were 42%, 42%, and 44% for $\theta_c = 30°$, 90°, and 180°, respectively. The frequency of transmitted photon bundles passing through one droplet was the largest at 46% for $\theta_c = 30°$ while it decreased to 7% for $\theta_c = 90°$, and 3% for $\theta_c = 180°$ This was due to the fact that, for a given projected surface area coverage f_A, the larger the contact angle the bigger the volume of droplets which contributed to stronger absorption. The maximum number of droplets through which transmitted photon bundles passed were 12, 6, and 2 for $\theta_c = 30°$, 90°, and 180°, respectively.

Finally, for all cases considered in Fig. 6 under normal incidence, less than 1% of the transmitted photon bundles passed through more than one droplet. However, for oblique incidence with $\theta_i = 60°$ more than 3% ($k_w = 10^{-6}$ and $k_d = 0$) passed through more than one droplets and successive internal reflection within droplets and the window could not be ignored (see Fig. S2 in Supplementary Material), unlike what has been assumed in previous studies [8,10,20].

3.4. Absorption by both window and droplets

Fig. 7 plots (a) the normal-hemispherical transmittance T_{nh} of a wet window and (b) the corresponding absorptance A_n as functions of contact angle θ_c when both the window ($k_w = 10^{-5}$) and

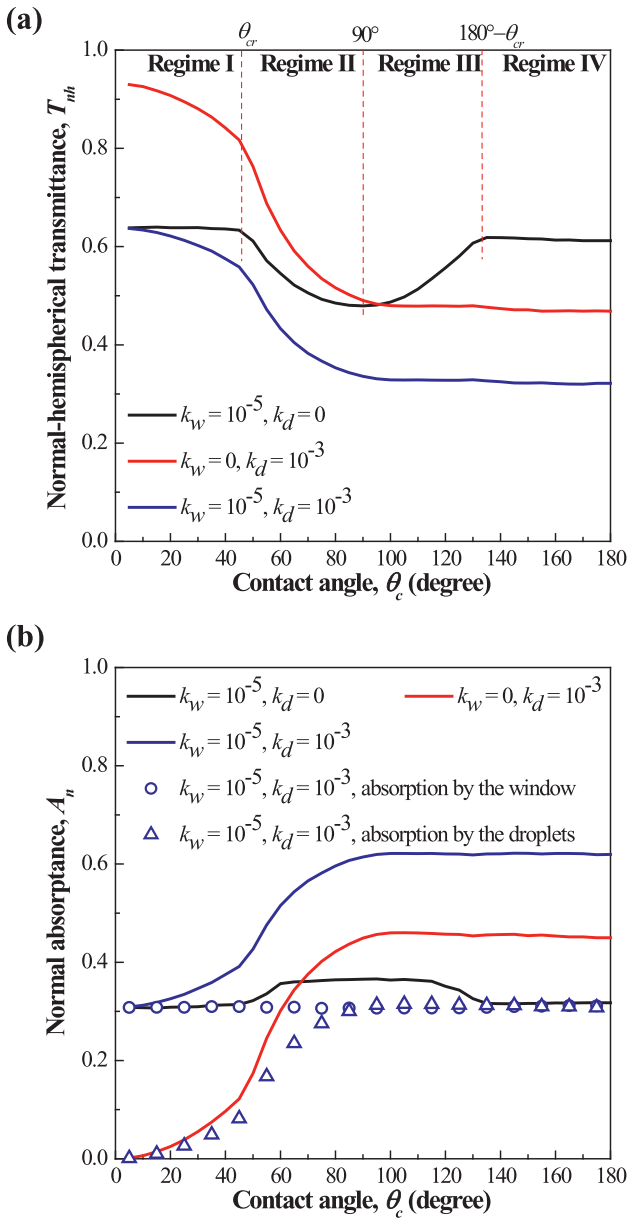

Fig. 7. (a) Normal-hemispherical transmittance and (b) normal absorptance as functions of droplet contact angle θ_c for wet windows with different values of k_w and k_d. The individual contributions of the window and droplets to absorption are also shown. The droplets were monodisperse with $d_m = 250\,\mu$m, $f_A = 55\%$, $\lambda = 1\,\mu$m, $n_w = 1.5$ and $n_d = 1.33$.

the droplets ($k_d = 10^{-3}$) were absorbing. For reference to previous simulations, the plots also show predictions when either the window or the droplets were nonabsorbing. Fig. 7(b) also shows the individual contributions of the semitransparent window and of the absorbing droplets to the overall normal absorptance. First, the normal-hemispherical transmittance T_{nh} for the semitransparent window and absorbing droplets ($k_w = 10^{-5}$ and $k_d = 10^{-3}$) decreased with increasing contact angle θ_c, while the associated absorptance A_n increased. In addition, for contact angles $\theta_c < 20°$, T_{nh} and A_n were identical to those of the semitransparent window with nonabsorbing droplets ($k_w = 10^{-5}$ and $k_d = 0$). This can be attributed to the fact that absorption by the window dominated and was independent of droplet contact angle for small contact angles, as evident in Fig. 7(b). By contract, the contribution of droplets to the overall absorption was negligible for small contact angles

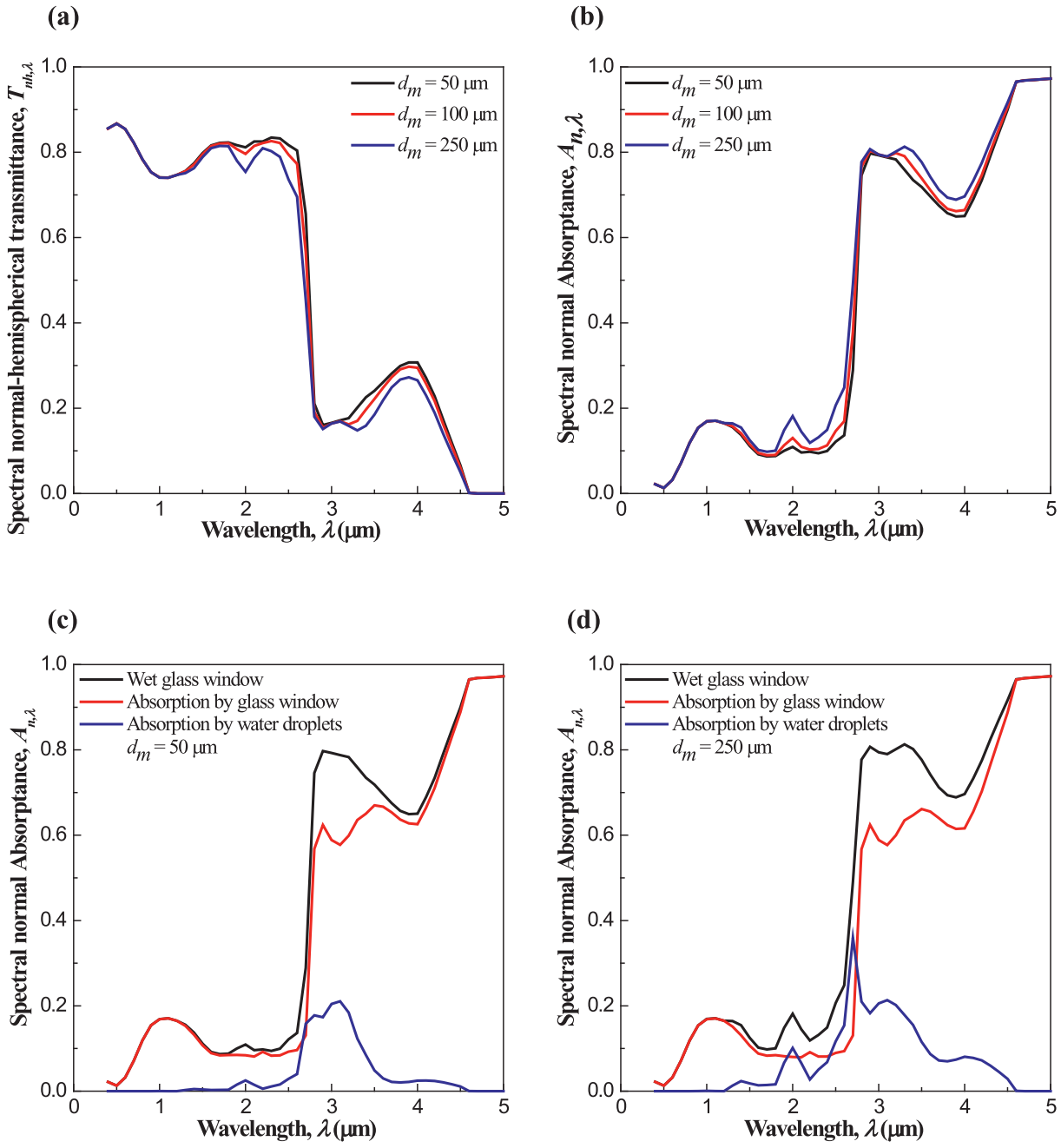

Fig. 8. Effect of monodisperse droplet size on the spectral normal-hemispherical transmittance and spectral normal absorptance for a 3 mm thick soda-lime silicate glass window with monodisperse water droplets ordered in a hexagonal pattern with $\theta_c = 50.9°$ and $f_A = 55\%$. (a) Spectral normal-hemispherical transmittance. (b) Spectral normal absorptance. (c) Spectral normal absorptance of wet glass window and contributions of absorption by the glass window and by water droplets for $d_m = 50\,\mu$m. (d) Spectral normal absorptance of wet glass window and contributions of absorption by the glass window and by water droplets for $d_m = 250\,\mu$m.

and increased with contact angle to reach a plateau for $\theta_c > 90°$ Interestingly, the contribution of droplets to the total absorption increased with increasing contact angle while that of the window remained independent of contact angle.

3.5. Glass window with condensed water droplets: from visible to mid-IR

Figs. 8(a) and 8(b) show respectively the spectral normal-hemispherical transmittance and the spectral normal absorptance of a 3 mm thick soda-lime silicate glass window with monodisperse water droplets of diameter $d_m = 50\,\mu$m, $100\,\mu$m, and $250\,\mu$m with contact angle $\theta_c = 50.9°$ corresponding to the contact angle of water droplets on an unclean glass window [1], and droplet projected surface area coverage $f_A = 55\%$. Note that, as previously demonstrated, the droplet spatial distribution had a slight effect on the transmittance and absorptance while their mean diameter d_m has a stronger effect than the standard deviation σ of their size distribution (see Fig. 4). Figs. 8(c) and 8(d) show the corresponding contributions to the spectral absorptance of the absorption by the glass window and by the water droplets of diameter $d_m = 50\,\mu$m and $250\,\mu$m, respectively.

Fig. 8 indicates that, for a given droplet projected surface area coverage f_A, (i) the spectral normal-hemispherical transmittance $T_{nh,\lambda}$ significantly decreased and (ii) the spectral normal absorptance $A_{n,\lambda}$ significantly increased with increasing droplet diame-

ter for wavelength λ in the spectral windows 1.8–2.7 μm and 3.1–4.6 μm. This was due to the fact that the larger the water droplets, the larger the amount of radiation they absorbed. However, the droplet diameter had negligible effect in the spectral ranges 0.4–1.8 μm, 2.7–3.1 μm, and beyond 4.6 μm. In the spectral range 0.4–1.8 μm, the absorption index $k_{d,\lambda}$ of water was so small that almost no photons were absorbed by the droplets. Instead, absorption was due only to the glass window. The four optical regimes previously discussed [10] (Fig. 5) and Eq. (16) prevailed. On the other hand, in the wavelength range 2.7–3.1 μm, photons entering the water droplets were all absorbed. Then, the non-zero transmittance was attributed to photons transmitted through the dry area of the glass window and depended only on droplet projected surface area coverage and was independent of droplet diameter. Then, Eq. (17) prevailed. For wavelength larger than 4.6 μm, photons transmitted through the air/window interface were all absorbed by the glass window and transmittance vanished.

4. Conclusion

This study numerically investigated light transfer through semitransparent windows with absorbing cap-shaped droplets condensed on their backside. It considered monodisperse droplets ordered in a hexagonal pattern or randomly distributed as well as randomly distributed polydisperse droplets with contact angle up to 180° The normal-hemispherical transmittance and normal absorptance of the wet window were predicted by Monte Carlo ray-tracing method after careful validation. The spatial distribution of the droplets had a slight effect on the normal-hemispherical transmittance. However, the normal-hemispherical transmittance decreased strongly with increasing size and polydispersity of *absorbing* droplets, unlike what was observed for *nonabsorbing* droplets [10]. The normal-hemispherical transmittance of semitransparent window supporting weakly absorbing droplets featured four distinct optical regimes defined based on the contact angle and the critical angle for total internal reflection at droplet/air interface, as previously observed [10]. However, the four optical regimes were no longer apparent for strongly absorbing droplets. Instead, the normal-hemispherical transmittance of wet window decreased with increasing contact angle for $\theta_c < 90°$ and remained constant and independent of the droplets' absorption index, mean diameter, and contact angle for $\theta_c \geq 90°$. Analytical expressions for the normal-hemispherical transmittance were provided in the asymptotic cases when (1) the droplets were nonabsorbing with any contact angles θ_c, and (2) the droplets were strongly absorbing with contact angle $\theta_c > 90°$. Finally, the spectral normal-hemispherical transmittance and absorptance of the practical case of a 3 mm thick glass window supporting condensed water droplets were predicted between 0.4 and 5 μm. These results can be used in the design and material selection of greenhouses, solar desalination systems, and photobioreactors in order to maximize their productivity as well as for their thermal management.

Acknowledgment

This study was financially supported by National Natural Science Foundation of China (No. 51406006) and by the China Scholarship Council (No. 201506025015).

Supplementary materials

Supplementary material associated with this article can be found, in the online version, at doi:10.1016/j.jqsrt.2017.06.016.

References

[1] Briscoe BJ, Galvin KP. The effect of surface fog on the transmittance of light. Sol Energy 1991;46:191–7.
[2] Pollet IV, Pieters JG. Condensation and radiation transmittance of greenhouse cladding materials, part 3: results for glass plates and plastic films. J Agric Eng Res 2000;77:419–28.
[3] Geoola F, Kashti Y, Peiper UM. A model greenhouse for testing the role of condensation, dust and dirt on the solar radiation transmissivity of greenhouse cladding materials. J Agric Eng Res 1998;71:339–46.
[4] Geoola F, Kashti Y, Levi A, Brickman R. Quality evaluation of anti-drop properties of greenhouse cladding materials. Polym Test 2004;23:755–61.
[5] Cemek B, Demir Y. Testing of the condensation characteristics and light transmissions of different plastic film covering materials. Polym Test 2005;24:284–9.
[6] Hsieh C, Rajvanshi AK. The effect of dropwise condensation on glass solar properties. Sol Energy 1977;19:389–93.
[7] Pieters JG, Deltour J, Debruyckere M. Light transmission through condensation on glass and polyethylene. Agric For Meteorol 1997;85:51–62.
[8] Tow EW. The antireflective potential of dropwise condensation. J Opt Soc Am A Optics Image Sci Vision 2014;31:493–9.
[9] Pruvost J, Leborgne F, Artu A, Cornet JF, Legrand J. Industrial photobioreactors and scale-up concepts. Photobioreaction engineering, 48; 2016. Special Issue of Advances Chemical Engineering.
[10] Zhu K, Huang Y, Pruvost J, Legrand J, Pilon L. Transmittance of transparent windows with nonabsorbing cap-shaped droplets condensed on their backside. J Quant Spectrosc Radiat Transfer 2017;194:98–107.
[11] Chaibi MT, Jilar T. Effects of a solar desalination module integrated in a greenhouse roof on light transmission and crop growth. Biosyst Eng 2005;90:319–30.
[12] De Gennes PG, Brochard-Wyart F, Quéré D. Capillarity and wetting phenomena: drops, bubbles, pearls, waves. Springer Science & Business Media; 2013.
[13] Bell RJ, Armstrong KR, Nichols CS, Bradley RW. Generalized laws of refraction and reflection. J Opt Soc Am 1969;59:187–9.
[14] Harpole GM. Radiative absorption by evaporating droplets. Int J Heat Mass Tran 1980;23:17–26.
[15] Chang PCY, Walker JG, Hopcraft KI. Ray tracing in absorbing media. J Quant Spectrosc Radiat Transfer 2005;96:327–41.
[16] Howell JR, Menguč MP, Siegel R. Thermal radiation heat transfer. 5th ed. Boca Raton: CRC Press; 2015.
[17] Modest MF. Radiative heat transfer. San Diego, CA: Academic Press; 2003.
[18] Rubin M. Optical properties of soda lime silica glasses. Sol Energy Mater 1985;12:275–88.
[19] Hale GM, Querry MR. Optical constants of water in the 200 nm to 200 μm wavelength region. Appl Opt 1973;12:555–63.
[20] Pieters JG. Interaction effects in simulating the light transmission through condensation drops on greenhouse covers. Trans ASAE 1997;40:1463–5.